34th Annual International Conference of the IEEE EMBS
San Diego, California USA, 28 August - 1 September, 2012

A Computational Multiscale Model of Glioblastoma Growth: Regulation of Cell Migration and Proliferation via microRNA-451, LKB1 and AMPK

Tina A. Schuetz[1,2], Stefan Becker[1,3], Andreas Mang[1], Alina Toma[1,3], Thorsten M. Buzug[1]

Abstract— **A new computational multiscale model of glioblastoma growth is introduced. This model combines an agent-based model for representing processes on the cellular level with a molecular interaction network for each cell on the subcellular scale. The network is based on recently published work on the interaction of microRNA-451, LKB1 and AMPK in the regulation of glioblastoma cell migration and proliferation. We translated this network into a mathematical description by the use of 17 ordinary differential equations. In our model, we furthermore establish a link from the molecular interaction network of a single cell to cellular actions (e.g. chemotactic movement) on the microscopic level. First results demonstrate that the computational model reproduces a tumor cell development comparable to that observed in *in vitro* experiments.**

I. INTRODUCTION

The present work introduces a novel computational model of glioblastoma (GB) growth. GB account for about one half of all gliomas (tumors arising from glial cells), and thus for 10% of all brain tumors in adults [1]. Despite all effort in therapy research the median survival is about 12 months [2].

Many cancer cells utilize glucose to pursue proliferation [3]. Under unfavorable glucose conditions they migrate to more beneficial sites to avoid metabolic stress. Godlewski et al. [4] showed that the microRNA-451 (miR-451) regulates GB cell migration and proliferation in response to different glucose conditions. MicroRNAs are short (about 22 nucleotides long) non-coding RNAs. They regulate the expression of about 60% of all human genes at the posttranscriptional level and microRNA dysregulation was found to be directly involved in the development of human cancer [5].

Godlewski et al. [4] discovered that the level of miR-451 in GB cells is elevated under normal glucose conditions and decreased in a low glucose environment. Furthermore, they showed that miR-451 targets the mRNA of MO25 (mouse protein 25) that forms a complex with LKB1 (liver kinase B1) and STRAD (sterile-20-related adaptor) [6]. The LKB1-MO25-STRAD complex acts as a kinase for AMPK (AMP activated protein kinase) and AMPK related kinases, such as MARK3 (MAP/microtubule affinity regulating kinase), thus increasing their activity by a factor of $100-150$ [7]. MARK3 plays a role in cell migration through regulating cell polarity. AMPK influences cell proliferation via mTOR signaling and is dephosphorylated if the AMP:ATP ratio is low, i.e. under medium to high glucose conditions. Active AMPK acts as a kinase for TSC2 (tuberous sclerosis complex 2) phosphorylation, which in turn inhibits Rheb (Ras homologue enriched in brain). Active Rheb has the ability to activate mTORC1 (mammalian target of rapamycin complex 1) [8]. Additionally, AMPK phosphorylates raptor and in doing so inhibits the activtity of mTORC1 [9]. mTORC1 can regulate the cell cycle, and thus proliferation, through the initiation of protein synthesis for cell growth and division [10]. Therefore, miR-451 establishes a direct link between a cell's glucose level and its decision for migration or proliferation.

Computational modeling of tumor growth aims at gaining a better understanding of the underlying biological processes and at aiding the improvement and development of therapies. Depending on the processes under investigation models on the macroscopic, the cellular or molecular scale as well as covering multiple scales can be employed [11], [12], [13].

Here, a molecular interaction network (mathematically expressed by means of ordinary differential equations (ODEs)) is developed that represents the processes described by Godlewski et al. [4] on the subcellular scale. Based on the multiscale modeling approach introduced by Athale et al. [14] the molecular level is coupled with the cellular one by equipping each individual cell (represented as the agents of an agent-based model (ABM)) with the molecular interaction network. This allows us to study *in silico* the spatio-temporal dynamics of the early GB growth phase in a comparable manner to *in vitro* experiments. In particular it is possible to compare the tumor development under different glucose conditions. Our first results show, that our computational model is able to reproduce the results obtained from biological experiments.

II. METHODS

Our model covers aspects on the subcellular scale (energy dependent decision for a migratory or proliferating phenotype) as well as on the cellular level, such as chemotaxis. This is done by combining an ABM, where each agent represents a biological cell, with a molecular interaction network that is given by 17 ODEs for each individual agent.

A. Subcellular scale: Molecular Interaction Network

Within each individual cell the interaction of the different relevant molecules (RNAs, proteins, glucose) is modeled

[1]The authors are with the Institute of Medical Engineering, University of Luebeck, 23562 Luebeck, Germany {schuetz, buzug} at imt.uni-luebeck.de

[2]T. A. Schuetz is with the Graduate School for Computing in Medicine and Life Sciences, University of Luebeck, 23562 Luebeck, Germany

[3]S. Becker and A. Toma are with the Centre of Excellence for Technology and Engineering in Medicine (TANDEM), 23562 Luebeck, Germany

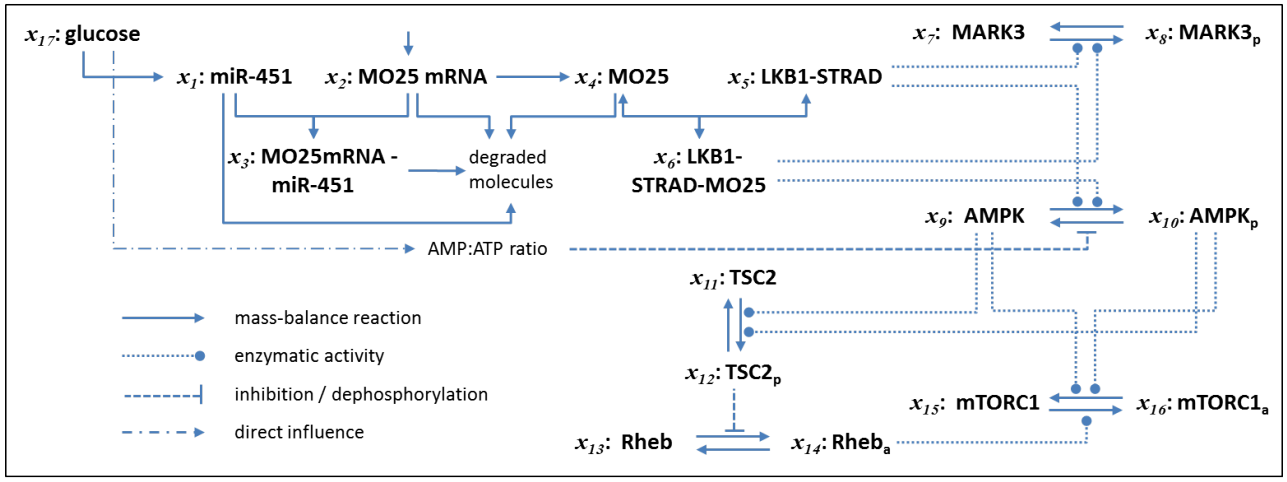

Fig. 1. The molecular interaction network with that each cell is equipped.

by mass-balance reactions and Michaelis-Menten equations for the enzyme kinetics. In total 17 molecular species are involved whose concentrations constitute the 17 variables of the system which are governed by 17 ODEs. The interaction network is shown in Fig. 1 and consists of the following elements:

MiR-451 (x_1) inhibits translation of MO25 mRNA (x_2) into protein (x_4) by binding and each of the components can be degraded. MO25 binds to LKB1 and STRAD (x_5) to form an active complex (x_6):

$$\begin{aligned}
\frac{\mathrm{d}x_1}{\mathrm{d}t} &= k_1 \cdot x_{17} - k_2 \cdot x_1 \cdot x_2 - k_3 \cdot x_1,\\
\frac{\mathrm{d}x_2}{\mathrm{d}t} &= k_4 - k_2 \cdot x_1 \cdot x_2 - k_6 \cdot x_2,\\
\frac{\mathrm{d}x_3}{\mathrm{d}t} &= k_2 \cdot x_1 \cdot x_2 - k_5 \cdot x_3,\\
\frac{\mathrm{d}x_4}{\mathrm{d}t} &= k_7 \cdot x_2 - k_8 \cdot x_4 - k_9 \cdot x_4 \cdot x_5 + k_{10} \cdot x_6,\\
\frac{\mathrm{d}x_5}{\mathrm{d}t} &= -k_9 \cdot x_4 \cdot x_5 + k_{10} \cdot x_6,\\
\frac{\mathrm{d}x_6}{\mathrm{d}t} &= k_9 \cdot x_4 \cdot x_5 - k_{10} \cdot x_6.
\end{aligned}$$

LKB1 phosphorylates MARK3 (x_7) and AMPK (x_9):

$$\begin{aligned}
\frac{\mathrm{d}x_7}{\mathrm{d}t} &= k_{11} \cdot x_8 - \frac{k_{12}^{c1} \cdot x_5 \cdot x_7}{k_{12}^{m1} + x_7} + \frac{k_{12}^{c2} \cdot x_6 \cdot x_7}{k_{12}^{m2} + x_7},\\
\frac{\mathrm{d}x_8}{\mathrm{d}t} &= -k_{11} \cdot x_8 + \frac{k_{12}^{c1} \cdot x_5 \cdot x_7}{k_{12}^{m1} + x_7} + \frac{k_{12}^{c2} \cdot x_6 \cdot x_7}{k_{12}^{m2} + x_7},\\
\frac{\mathrm{d}x_9}{\mathrm{d}t} &= -\frac{k_{13}^{c1} \cdot x_5 \cdot x_9}{k_{13}^{m1} + x_9} + \frac{k_{13}^{c2} \cdot x_6 \cdot x_9}{k_{13}^{m2} + x_9} + \frac{k_{14}^{i} \cdot k_{14} \cdot x_{10}}{k_{14}^{i} + S_1},\\
\frac{\mathrm{d}x_{10}}{\mathrm{d}t} &= \frac{k_{13}^{c1} \cdot x_5 \cdot x_9}{k_{13}^{m1} + x_9} + \frac{k_{13}^{c2} \cdot x_6 \cdot x_9}{k_{13}^{m2} + x_9} - \frac{k_{14}^{i} \cdot k_{14} \cdot x_{10}}{k_{14}^{i} + S_1}.
\end{aligned}$$

AMPK regulates mTORC1 activity (x_{16}) on the one hand immediately through raptor binding and on the other hand via TSC2 (x_{11}) phosphorylation and Rheb (x_{13}) activation:

$$\begin{aligned}
\frac{\mathrm{d}x_{11}}{\mathrm{d}t} &= -\frac{k_{15}^{c1} \cdot x_9 \cdot x_{11}}{k_{15}^{m1} + x_{11}} - \frac{k_{15}^{c2} \cdot x_{10} \cdot x_{11}}{k_{15}^{m2} + x_{11}} + k_{16} \cdot x_{12},\\
\frac{\mathrm{d}x_{12}}{\mathrm{d}t} &= \frac{k_{15}^{c1} \cdot x_9 \cdot x_{11}}{k_{15}^{m1} + x_{11}} + \frac{k_{15}^{c2} \cdot x_{10} \cdot x_{11}}{k_{15}^{m2} + x_{11}} - k_{16} \cdot x_{12},\\
\frac{\mathrm{d}x_{13}}{\mathrm{d}t} &= -\frac{k_{17}^{i} \cdot k_{17} \cdot x_{13}}{k_{17}^{i} + x_{12}} + k_{18} \cdot x_{14},\\
\frac{\mathrm{d}x_{14}}{\mathrm{d}t} &= \frac{k_{17}^{i} \cdot k_{17} \cdot x_{13}}{k_{17}^{i} + x_{12}} - k_{18} \cdot x_{14},\\
\frac{\mathrm{d}x_{15}}{\mathrm{d}t} &= \frac{k_{19}^{c1} \cdot x_9 \cdot x_{16}}{k_{19}^{m1} + x_{16}} + \frac{k_{19}^{c2} \cdot x_{10} \cdot x_{16}}{k_{19}^{m2} + x_{16}} - \frac{k_{20}^{c} \cdot x_{14} \cdot x_{15}}{k_{20}^{m} + x_{15}},\\
\frac{\mathrm{d}x_{16}}{\mathrm{d}t} &= -\frac{k_{19}^{c1} \cdot x_9 \cdot x_{16}}{k_{19}^{m1} + x_{16}} - \frac{k_{19}^{c2} \cdot x_{10} \cdot x_{16}}{k_{19}^{m2} + x_{16}} + \frac{k_{20}^{c} \cdot x_{14} \cdot x_{15}}{k_{20}^{m} + x_{15}}.
\end{aligned}$$

Glucose is constantly consumed by the cells:

$$\frac{\mathrm{d}x_{17}}{\mathrm{d}t} = -r_n.$$

The reaction parameters and initial variable values were taken from the literature [4], [15], [16] or are estimates if no data were available. They are summarized in table I (estimates are marked by a *) and table II.

TABLE I

MOLECULAR SPECIES AND RESPECTIVE INITIAL CONDITIONS.

Species	Name	Initial value	Unit
x_1	miR451	3.8728×10^2	pmol l^{-1}
x_2	MO25 mRNA	3	pmol l^{-1}
x_3	MO25 miRNA bound *	0	pmol l^{-1}
x_4	MO25	5×10^4	pmol l^{-1}
x_5	LKB1-STRAD *	5×10^4	pmol l^{-1}
x_6	LKB1-STRAD-MO25 *	5×10^4	pmol l^{-1}
x_7	MARK3	1.2897×10^3	pmol l^{-1}
x_8	MARK3 phosphorylated	0	pmol l^{-1}
x_9	AMPK	6.709×10^3	pmol l^{-1}
x_{10}	AMPK phosphorylated	0	pmol l^{-1}
x_{11}	TSC2	4.4333×10^1	pmol l^{-1}
x_{12}	TSC2 phosphorylated	0	pmol l^{-1}
x_{13}	Rheb	$1.512\,66 \times 10^4$	pmol l^{-1}
x_{14}	Rheb active	0	pmol l^{-1}
x_{15}	mTOR C1	4.4087×10^2	pmol l^{-1}
x_{16}	mTOR C1 active	0	pmol l^{-1}
x_{17}	Glucose	0.3 to 4.5	g l^{-1}

TABLE II

PARAMETERS FOR REACTIONS.

Parameter	Value	Unit
k_1	6×10^{-7}	s^{-1}
k_2	3×10^{-2}	s^{-1}
k_3	3×10^{1}	$\mathrm{pmol\,l^{-1}\,s^{-1}}$
k_4	8.7498	s^{-1}
k_5	3.6×10^{2}	s^{-1}
k_6	1.0467×10^{-2}	s^{-1}
k_7	1.4065×10^{1}	s^{-1}
k_8	6.4167×10^{-3}	$\mathrm{pmol\,l^{-1}\,s^{-1}}$
k_9	6×10^{-2}	s^{-1}
k_{10}	3.6×10^{2}	s^{-1}
k_{11}	6×10^{-1}	s^{-1}
k_{12}^{m1}	5×10^{3}	$\mathrm{pmol\,l^{-1}}$
k_{12}^{c1}	1×10^{-1}	$\mathrm{pmol^{-1}\,l^{-1}\,s^{-1}}$
k_{12}^{m2}	5×10^{3}	$\mathrm{pmol\,l^{-1}}$
k_{12}^{c2}	1	$\mathrm{pmol^{-1}\,l^{-1}\,s^{-1}}$
k_{13}^{m1}	5×10^{2}	$\mathrm{pmol\,l^{-1}}$
k_{13}^{c1}	1.8×10^{1}	$\mathrm{pmol^{-1}\,l^{-1}\,s^{-1}}$
k_{13}^{m2}	5×10^{2}	$\mathrm{pmol\,l^{-1}}$
k_{13}^{c2}	1.8×10^{2}	$\mathrm{pmol^{-1}\,l^{-1}\,s^{-1}}$
k_{14}^{i}	6×10^{-1}	$\mathrm{pmol\,l^{-1}}$
k_{14}	6×10^{2}	$\mathrm{pmol^{-1}\,l^{-1}\,s^{-1}}$
k_{15}^{m1}	1×10^{2}	$\mathrm{pmol\,l^{-1}}$
k_{15}^{c1}	6×10^{-2}	$\mathrm{pmol^{-1}\,l^{-1}\,s^{-1}}$
k_{15}^{m2}	1×10^{2}	$\mathrm{pmol\,l^{-1}}$
k_{15}^{c2}	6	$\mathrm{pmol^{-1}\,l^{-1}\,s^{-1}}$
k_{16}	3.6×10^{2}	s^{-1}
k_{17}^{i}	5	$\mathrm{pmol\,l^{-1}}$
k_{17}	3.6×10^{2}	$\mathrm{pmol^{-1}\,l^{-1}\,s^{-1}}$
k_{18}	3.6×10^{2}	s^{-1}
k_{19}^{m1}	1×10^{2}	$\mathrm{pmol\,l^{-1}}$
k_{19}^{c1}	3.6×10^{-1}	$\mathrm{pmol^{-1}\,l^{-1}\,s^{-1}}$
k_{19}^{m2}	1×10^{2}	$\mathrm{pmol\,l^{-1}}$
k_{19}^{c2}	3.6×10^{1}	$\mathrm{pmol^{-1}\,l^{-1}\,s^{-1}}$
k_{20}^{m}	1.5104×10^{3}	$\mathrm{pmol\,l^{-1}}$
k_{20}^{c}	1.08×10^{2}	$\mathrm{pmol^{-1}\,l^{-1}\,s^{-1}}$
r_n	1.17×10^{-2}	$\mathrm{mmol\,l^{-1}\,s^{-1}}$

B. Cellular scale: Chemotaxis

A regular 200×200 grid representing an area of $3\,\mathrm{mm} \times 3\,\mathrm{mm}$ can contain at each grid point one biological cell of the size $15\,\mu\mathrm{m} \times 15\,\mu\mathrm{m}$. Initially a constant glucose concentration is assumed on the whole grid. Over time, glucose is consumed by the cells ($\frac{\mathrm{dx_{17}}}{\mathrm{dt}} = -r_n$) and diffuses through the grid as mathematically described by the following partial differential equation:

$$\frac{\partial x_{17}}{\partial t} = D\ \nabla^2 x_{17}, \tag{1}$$

where D is the diffusion coefficient for glucose.

If a cell is selected to migrate, its movement will follow the gradient of a chemotactic agent. Since glucose is already part of the model and acts as an attractor for tumor cells [17], the new cell position is chosen as the empty neighbor with the highest glucose concentration.Also, if a cell proliferates, its daughter cell is positioned according to the same rule.

C. Coupling the Molecular and Cellular Scale

To combine the above two described models an ABM approach is applied. This enables the assessment of the effects of the molecular scale on the tumor development at the cellular level. The individual cells form the agents. Their action rules are given by 1.) the decision for a phenotype according to the molecular interaction network and 2.) the movement according to the chemotaxis condition.

In each time step the cells are processed in a random order to avoid any unnatural pattern formation. For each cell first the molecular interaction network will be evaluated. Then, linearly dependent on the concentrations of phosphorylated MARK3 (x_8) and active mTORC1 (x_{16}) a probability for the cell's phenotype (proliferating, migrating or quiescent) is determined. Finally, depending on the phenotype, the daughter cell is placed in the cell's neighborhood, the cell is moved to a more attractive position or the cell is kept unchanged as a quiescent cell. After all cells are updated the glucose levels are refreshed by evaluating (1).

III. RESULTS

Godlewski et al. [4] showed the results of two *in vitro* experiments of glioblastoma spheroid migration under different glucose conditions. They compare the tumor development under a glucose level of $2.25\,\mathrm{g\,l^{-1}}$ to the development if the glucose level is low ($0.3\,\mathrm{g\,l^{-1}}$). They observe a significantly increased migration under low glucose conditions.

To evaluate our model we emulate the conditions of the migration assay. Initially, we place 797 tumor cells in the center of the grid (representing a circular area with a radius of $240\,\mu\mathrm{m} = 16$ cells). The simulation is run according to the description in section II with one time step corresponding to one hour. The system of ODEs is solved numerically by a four-stage Runge-Kutta scheme and the PDE is solved with a finite-difference method.

To compare the results of our model to the *in vitro* experiments we simulated the development of the *in silico* tumor with an initial condition of $0.3\,\mathrm{g\,l^{-1}}$ glucose and $2.25\,\mathrm{g\,l^{-1}}$ glucose. Fig. 2(a) shows the results of these experiments after a simulated period of 6 hours. The migratory area of the $0.3\,\mathrm{g\,l^{-1}}$ glucose simulation is indicated by the green dashed half circle and the blue solid half circle displays the migration zone of the $2.25\,\mathrm{g\,l^{-1}}$ glucose simulation. Proliferating cells are displayed in light gray, migrating cells are shown as dark gray and quiescent cells are color coded as black.

Additionally, Fig. 2(b) shows the spatio-temporal development of the tumor growth for the same two glucose settings (upper row: $0.3\,\mathrm{g\,l^{-1}}$, lower row: $2.25\,\mathrm{g\,l^{-1}}$). We stopped the simulations as soon as a tumor cell reached the boundary.

IV. DISCUSSION AND CONCLUSIONS

The *in vitro* experiment in Godlewski et al. [4] demonstrates that under low glucose conditions a tumor tends to migrate faster and further than under medium glucose conditions. The same observation can be made in the *in silico* experiments with our newly developed computational model. The comparison of the different glucose conditions in Fig. 2(a) shows that the migratory area of the tumor cells has a greater extend if the tumor is grown on a $0.3\,\mathrm{g\,l^{-1}}$ glucose medium as compared to a $2.25\,\mathrm{g\,l^{-1}}$ glucose medium.

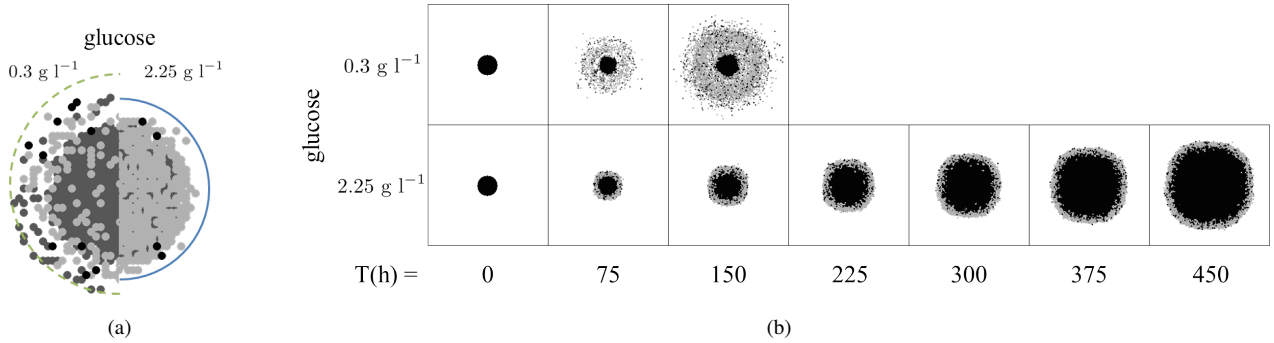

Fig. 2. (a) Comparison of results of *in silico* experiments under different initial glucose conditions (left: $0.3\,\mathrm{g\,l^{-1}}$, right: $2.25\,\mathrm{g\,l^{-1}}$) at T = 6 h. (b) The spatio-temporal development of the *in silico* tumor growth under different glucose conditions. For the *in silico* experiments in (a) and (b) the following color coding holds: black: quiescent cells; dark gray: migrating cells; light gray: proliferating cells.

Since a sufficient glucose supply is essential for the GB cell's proliferation potential, proliferation is significantly reduced under low glucose conditions. Due to nutrient consumption by the tumor cells, the glucose level is lower in the area where the tumor bulk is located. Thus, if the glucose supply is insufficient, tumor cells seek for a more advantageous environment by migrating away from the tumor bulk. On the other hand, if a tumor cell has enough glucose at its disposal, it has the ability to initiate proliferation such that there is no need for migration.

This behavior can also be observed in Fig. 2(b). Here the spatial tumor development over time is depicted for two different glucose levels until the first cell reaches the boundary. A medium glucose level ($2.25\,\mathrm{g\,l^{-1}}$, lower row in Fig. 2(b)) results in an evenly growing tumor that is very densely packed (29 571 cells in the last time step, T = 623 h) and exhibits a quiescent core surrounded by a rim of migrating and proliferating cells. In an environment containing less glucose ($0.3\,\mathrm{g\,l^{-1}}$, upper row in Fig. 2(b)) the tumor has a more diffusive character and dispreads faster (containing 5693 cells in the last time step, T = 158 h).

Overall, the results demonstrate that our computational model is capable of reproducing GB growth behavior as it is expected from the biological context. In particular under low glucose conditions, the simulated tumor exhibits a behavior that is essential for the aggressive character of GB tumors: Individual cells separate from the tumor bulk and invade the surrounding (healthy) micro environment.

This behavior is also seen in the results of Athale et al. [14]. However, in their work no specific *in vitro* experiment is emulated, but rather a general *in vivo* setting.

Our future research is directed towards a sensitivity analysis of the involved parameters. This analysis will allow us to identify parameters that have a crucial influence on the overall system behavior. Thus, these parameters will have to be estimated even more precisely and can be used to indicate potential new therapy targets.

ACKNOWLEDGMENT

We acknowledge the support of Germanys Excellence Initiative [DFG GSC 235/1] (T. A. Schuetz), and the European Union and the State Schleswig-Holstein (Programme for the Future-Economy: 122-09-024) (A. Toma & S. Becker).

REFERENCES

[1] A. M. Dubuc, S. Mack *et al.*, *Cancer Epigenetics*, ser. Methods in Molecular Biology. Humana Press, 2012, vol. 863, no. 2, ch. 8: The epigenetcs of brain tumors, pp. 139–153.
[2] D. Krex, B. Klink *et al.*, "Long-term survival with glioblastoma multiforme," *Brain*, vol. 130, no. 10, pp. 2596–2606, 2007.
[3] J.-W. Kim and C. V. Dang, "Cancer's molecular sweet tooth and the warburg effect," *Cancer Res.*, vol. 66, no. 18, pp. 8927–8930, 2006.
[4] J. Godlewski, M. O. Nowicki *et al.*, "MicroRNA-451 regulates LKB1/AMPK signaling and allows adaptation to metabolic stress in glioma cells," *Mol. Cell*, vol. 37, pp. 620–632, 2010.
[5] A. Esquela-Kerscher, *MicroRNAs in development and cancer*, ser. Molecular Medicine and Medicinal Chemistry. Imperial College Press, 2011, vol. 1, ch. 6: MicroRNAs function as tumor suppressor genes and oncogenes, pp. 149–184.
[6] J. Boudeau, A. F. Baas *et al.*, "MO25α/β interact with STRADα/β enhancing their ability to bind, activate and localize LKB1 in the cytoplasm," *EMBO J.*, vol. 22, no. 19, pp. 5102–5114, 2003.
[7] J. M. Lizcano, O. Gransson *et al.*, "LKB1 is a master kinase that activates 13 kinases of the AMPK subfamily, including MARK/PAR-1," *EMBO J.*, vol. 23, pp. 833–843, 2004.
[8] K. Inoki, Y. Li, T. Xu, and K.-L. Guan, "Rheb GTPase is a direct target of TSC2 GAP activity and regulates mTOR signaling," *Genes Dev.*, vol. 17, pp. 1829–1834, 2003.
[9] D. M. Gwinn, D. B. Shackelford *et al.*, "AMPK phosphorylation of raptor mediates a metabolic checkpoint," *Mol. Cell*, vol. 30, pp. 214–226, 2008.
[10] S. Wullschleger, R. Loewith, and M. N. Hall, "TOR signaling in growth and metabolism," *Cell*, vol. 124, pp. 471–484, 2006.
[11] N. Bellomo, M. Chaplain, and E. D. Angelis, Eds., *Selected Topics in Cancer Modeling - Genesis, Evolution, Immune Competition and Therapy*. Birkhuser, 2008.
[12] N. Bellomo, N. K. Li, and P. K. Maini, "On the foundations of cancer modelling: Selected topics, speculations, and perspectives," *Math. Models Methods Appl. Sci.*, vol. 18, no. 4, pp. 593–646, 2008.
[13] T. S. Deisboeck and G. S. Stamatakos, Eds., *Multiscale Cancer Modeling*. Chapman & Hall / CRC, 2011.
[14] C. Athale, Y. Mansury, and T. S. Deisboeck, "Simulating the impacts of a molecular 'decision-process' on cellular phenotype and multicellular patterns in brain tumors," *J. Theor. Biol.*, vol. 233, no. 4, pp. 469–481, 2005.
[15] B. Schwanhaeusser, D. Busse *et al.*, "Global quantification of mammalian gene expression control." *Nature*, vol. 473, no. 5, pp. 337–42, 2011.
[16] L. Zhang, C. A. Athale, and T. S. Deisboeck, "Development of a three-dimensional multiscale agent-based tumor model: Simulating gene-protein interaction profiles, cell phenotypes and multicellular patterns in brain cancer," *J. Theor. Biol.*, vol. 244, pp. 98–107, 2007.
[17] L. M. Sander and T. S. Deisboeck, "Growth patterns of microscopic brain tumors," *Phys. Rev. E*, vol. 66, p. 051901, 2002.